Phase Behavior of an ABC Triblock Copolymer Blended with A and C Homopolymers

Masaaki Sugiyama,† Terri A. Shefelbine, Martin E. Vigild,‡ and Frank S. Bates*

Department of Chemical Engineering and Materials Science, University of Minnesota, Minneapolis, Minnesota 55455

Received: May 22, 2001; In Final Form: October 1, 2001

The structures of ternary blends composed of a nearly symmetric poly(styrene-*b*-isoprene-*b*-dimethylsiloxane) (SID) triblock copolymer (volume fractions of S/I/D = 0.20/0.59/0.21, M_n = 40 000 g/mol) and equal volume fractions of low-molecular-weight polystyrene (M_n = 2360 g/mol) and poly(dimethylsiloxane) (M_n = 2200 g/mol) are investigated by small-angle X-ray and neutron scattering and transmission electron microscopy. When the total homopolymer volume fraction exceeds 65%, the blend macroscopically separates into ordered homopolymer-poor and -rich regions. Between 45 and 65% homopolymer volume fraction, hexagonally packed core−shell cylinders form with PDMS cores and PI shells. Between 15 and 45% homopolymer volume fraction, a core−shell gyroid morphology is observed with PDMS cores and PI shells. These core−shell variations of the classical structures of diblock copolymers are attributed to a small asymmetry in segment−segment interaction parameters. The neat SID block copolymer has a new complex ordered microstructure.

Introduction

The self-assembled structures of block copolymers have fascinated researchers from both theoretical and applied perspectives for four decades. The thermodynamic balance between the segment−segment contact energy (χ) and chain-stretching-driven changes in entropy causes block copolymers to microphase separate into well-ordered structures below an order−disorder transition determined by the product χN, where N is the degree of polymerization. In the case of AB diblocks four stable ordered structures have been documented: lamellae, gyroids, cylinders, and spheres.[1,2] Most commercial applications of block copolymers, for example adhesives and thermoplastic elastomers, rely on the ability of these materials to order, and in some cases to disorder, at elevated temperatures to facilitate processing. However, promising new applications have been cited in the literature that could take advantage of the specific microstructures of these and other elegant microstructures of block copolymers including templates for nanofabrication,[3] encapsulation,[4] and low-k dielectric materials.[5]

To increase the diversity of possible applications, we have turned our attention to ABC triblock copolymers. Complex phases, such as gyroids, are especially attractive because properties such as permeability or conductivity are isotropic, eliminating the need to align the unit cell with the direction of interest during processing. To apply these structures commercially, the complex phase window must be easily accessible. In AB diblock copolymers, the complex gyroid phase appears over a 3−4% range in the volume fraction of each block and is not anticipated in the strong segregation region.[6] Blending block copolymers of different compositions or adding homopolymer to a block copolymer reduces the need to synthesize molecules of different compositions to access the gyroid phase in the weak to intermediate segregation regions.[7] Preliminary evidence for ABC triblock copolymers[8] suggests that the complex gyroid phase extends into a stronger segregation region, although the composition window likely is still relatively narrow. Because segregation strength is proportional to the product χN, the ability to access complex phases at higher segregation allows for the use of higher-molecular-weight materials, which have better mechanical properties. Understanding the phase behavior of ABC triblocks in the complex region is an important step in harnessing the diversity of ABC triblock structures for applications.

Unfortunately, mapping the phase diagram of ABC triblocks is tedious because of the large number of parameters defining their phase behavior. Blending homopolymers with triblocks changes the composition easily, but studies with AB diblock copolymer−homopolymer blends show that the morphologies observed in blends are not strictly equivalent to neat diblock copolymers in composition.[9] In addition, some morphologies are predicted to be thermodynamically stable in blends that are not stable in neat diblocks.[10] However, once a region of interest, such as a complex phase, is identified, corresponding neat triblock copolymers can be synthesized in that region to study the phase diagram of neat triblocks exactly.

The addition of homopolymers to block copolymers mimics the addition of oil and water to surfactants, soaps, and lipids. Prior experiments[11] have shown that mixtures of AB diblock copolymers and the corresponding A and B homopolymers produce nanoscale topologies that are familiar to the surfactant community, including spheres, cylinders, gyroids, and lamellae. Under symmetric conditions (equal amounts of equal-molecular-weight A and B homopolymers and a compositionally symmetric AB diblock that is approximately five times greater in molecular weight) the A/B/AB system also exhibits a bicontinuous microemulsion state[13] analogous to that documented in low-molecular-weight amphiphilic systems.[12] However, whereas the block copolymer mixture is characterized by a microemulsion channel over a wide temperature range, this disordered bicontinuous morphology is restricted to a narrow slice in composition and temperature in oil/water/surfactant systems. Recent theoretical considerations[14] suggest that ABC triblock copolymers when mixed with A and C homopolymers should form disordered

* To whom correspondence should be addressed (bates@cems.umn.edu).
† Current address: Department of Physics, Kyushu University, Fukuoka 812-8581, Japan (sugi8scp@mbox.nc.kyushu-u.ac.jp).
‡ Current address: Department of Chemical Engineering, Technical University of Denmark, 2800 Lyngby, Denmark.

10.1021/jp011959r CCC: $20.00
Published on Web 11/27/2001

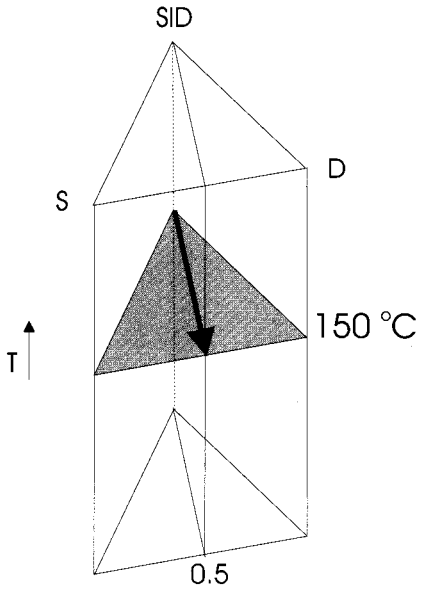

Figure 1. Phase prism for ABC triblock copolymers blended with A and C homopolymers. The temperature plane investigated is shaded, and the composition line of the experiments is marked with an arrow.

tricontinuous microemulsions with convoluted sheets of B polymer separating continuous domains of A and C. A variety of technological applications can be envisioned for such materials including their use as membranes and toughened plastics.

In terms of the general phase behavior of all ABC triblock systems, most morphologies can be classified according to the relative magnitude of the χ parameters.[15] Stadler and colleagues studied ABC triblocks with short middle blocks and χ parameters such that $\chi_{AC} < \chi_{AB} \approx \chi_{BC}$. For these polymers, contact between the A and C blocks is favorable, and the end blocks form the classical (diblock) domains, namely, lamellae, cylinders, and spheres, with various shapes of B block domains decorating the A−C interfaces.[16] In another class of systems, the χ parameter between the end blocks is the largest, $\chi_{AC} > \chi_{AB} \approx \chi_{BC}$. For these polymers, contact between the A and C blocks is the least favorable, and alternating structures form such as ABCCBA lamellae, hexagonally[17] and tetragonally[18] packed alternating cylinders, alternating spheres,[18] and alternating gyroids.[19] In the systems where the χ parameter between the end blocks and the middle block are asymmetric and the χ parameters between the end blocks is the largest, $\chi_{AC} > \chi_{BC} > \chi_{AB}$, there is spontaneous curvature toward one interface and formation of core−shell structures, such as core−shell cylinders[18] and core−shell gyroids.[8,20,21] Most ABC morphologies, with the notable exception of the knitting pattern,[22] are variations of the four classical structures of the AB diblock copolymers, whose specific form is determined by the relative χ parameters.

In this publication, we examine the phase behavior of blends of poly(styrene-*b*-isoprene-*b*-dimethylsiloxane) (SID) triblock copolymer with S/I/D volume fractions 0.20/0.59/0.21 and a molecular weight of 40 000 g/mol and equal amounts of low-molecular-weight polystyrene and poly(dimethylsiloxane) up to 65 vol % homopolymer. A schematic of the phase diagram for this ternary system is shown in Figure 1, with the line of compositions studied here marked by an arrow. The χ parameters for this system at 150 °C are $\chi_{SI} = 0.06$,[23] $\chi_{ID} = 0.09$,[24] and $\chi_{SD} = 0.20$.[24] By analogy with AB diblock/homopolymer blends,[11] we expect to add a large amount of these low-molecular-weight homopolymers before bulk phase separation between a triblock copolymer and homopolymers occurs. The structure of each blend was investigated using a combination of small-angle X-ray scattering (SAXS), small-angle neutron scattering (SANS), and transmission electron microscopy (TEM).

Experimental Section

A. Synthesis of SID. The triblock copolymer used in this study was synthesized by sequential anionic polymerization. Styrene, isoprene, cyclohexane, and tetrahydrofuran were rigorously purified as described elsewhere.[25] Hexamethylcyclotrisiloxane (D_3) monomer was purified by dissolving the monomer in cyclohexane, passing it through a basic alumina column, and sparging the solution with ultra-high-purity argon for 30 min. The concentration of the resulting solution was measured with ^{1}H NMR spectroscopy. Styrene monomer (10.3 g) was initiated with *sec*-butyllithium in approximately 200 mL of cyclohexane at 38 °C and polymerized for 4 h. Next, the isoprene monomer (26.7 g) was added to the reaction mixture; within 2 min, the orange color of the polystyrenyllithium was extinguished, indicating crossover to polyisoprenyllithium. Isoprene was polymerized in cyclohexane at 40 °C with primarily the 4,1 microstructure.[26] After 4 h, the reaction mixture was cooled to 6 °C using an external ice bath, and then 300 mL of tetrahydrofuran was added to the reactor, which turned the solution yellow. Enough D_3 solution was then cannulated into the reactor to provide a 100% excess of D_3 (17.6 g). The yellow color disappeared within 10 min, indicating crossover to the lithium siloxylanoate anion. After allowing the D_3 to polymerize for 4 h at 20 °C, the reaction was terminated with an excess of chlorotrimethylsilane. The polymer was recovered by precipitation from a 1:1 volume mixture of 2-propanol and methanol. Excess D_3 was washed from the polymer with methanol, and the polymer was dried in a vacuum oven to constant weight. The yield was 45.1 g.

The chemical structure of the resulting polymer was characterized by gel permeation chromatography (GPC) and ^{1}H NMR spectroscopy. The polydispersity of this polymer was $M_w/M_n = 1.1$ relative to PS standards as determined using a Waters GPC fitted with Phenogel columns running with chloroform. From NMR spectroscopy the repeat unit molar fractions of styrene, isoprene, and dimethylsiloxane are 0.18, 0.4, and 0.24, respectively. Using published densities (at 140 °C) of the respective homopolymers,[27] these molar fractions convert to volume fractions of 0.20/0.59/0.21 for S/I/D, respectively. Also from NMR spectroscopy the estimated molecular weight (M_n) of the SID triblock is 42 000 g/mol, based on monomer-to-initiator methyl-group-integrated resonant intensities. The targeted molecular weight of this triblock was 40 000 g/mol based on the initiator-to-monomer ratio. This difference is within the experimental accuracy of the NMR technique for determining molecular weight (10%).

PDMS homopolymer was synthesized by anionic polymerization of D_3. D_3 was initiated by *sec*-butyllithium in cyclohexane, and then an equal volume of tetrahydrofuran was added to promote the polymerization. The room-temperature reaction was terminated after 4 h with an excess of chlorotrimethylsilane. Polymer was recovered by rotovaping the reaction solvents and extracting the polymer with methanol several times to remove excess D_3. Finally, the PDMS was dried overnight in a vacuum oven to remove remaining solvent. The polydispersity was found to be 1.1 relative to polystyrene standards. From NMR spectroscopy, the molecular weight (M_n) was calculated to be 2200 g/mol. The polystyrene homopolymer used for these experiments was purchased as a standard from Aldrich having a molecular weight of 2360 g/mol and a polydispersity of 1.06.

TABLE 1: S/I/SID Ternary Blends

code	ϕ_H[a]	ϕ_S[b]	ϕ_I[b]	ϕ_D[b]
A	0.000	0.200	0.590	0.210
B	0.097	0.229	0.533	0.238
C	0.207	0.264	0.468	0.268
D	0.299	0.290	0.414	0.297
E	0.352	0.303	0.382	0.315
F	0.394	0.317	0.358	0.326
G	0.454	0.337	0.322	0.341
H	0.500	0.347	0.295	0.358
I	0.546	0.367	0.268	0.365
J	0.596	0.378	0.239	0.383
K	0.653	0.397	0.205	0.399

[a] ϕ_H is the total homopolymer volume fraction. [b] ϕ_S, ϕ_I, and ϕ_D are total volume fractions of S, I, and D domains, respectively.

B. Preparation of Blended Samples. The compositions of the SID triblock and homopolymer blends were determined by weighing predetermined quantities of the three components. To reduce the number of adjustable parameters, the volume fractions of the two homopolymers were kept equal, i.e., $\phi_{HS} = \phi_{HD}$, where ϕ_{HS} and ϕ_{HD} are volume fractions of homopolymer PS and homopolymer PDMS, respectively. The total volume fraction of the homopolymers, $\phi_H = \phi_{HS} + \phi_{HD}$, is the only adjustable parameter in the experiments. The polymers were dissolved in toluene at a total polymer concentration of 5 wt %, and the solution was stirred for 1 h. Next, the blended samples were cast on a flat glass plate and dried slowly over the course of 3 weeks in a vessel having a high vapor pressure of toluene. After the residual toluene was removed by pre-annealing in a vacuum oven at 150 °C and 0.2 Torr, the samples were sealed under vacuum in an ampule and annealed in an oil bath at 150 °C for 1 week. Finally, the annealed samples were quenched in liquid nitrogen to trap the high-temperature structure. The composition of each blend was verified by NMR spectroscopy and found to agree with the composition by weight within experimental error. We covered the range of ϕ_H from 0 to 0.65. The samples are listed in Table 1.

C. Small-Angle X-ray Scattering. We used a SAXS diffractometer at the Institute of Technology Characterization Facility at the University of Minnesota. The incident beam with a wavelength of 1.54 Å was focused with two Franks mirrors, and the scattered X-rays were detected with a two-dimensional position-sensitive detector (2-D PSD). The distance between the sample position and the detector was 2.30 m, and the magnitude of the scattering vector q ranged from 9.0×10^{-3} to 1.0×10^{-1} Å^{-1}.

We performed three types of SAXS experiments:

(1) Standard SAXS Experiment. SAXS intensities were recorded for 1-mm-thick pieces of all samples listed in Table 1. Scattering intensity was accumulated on the 2-D PSD and then azimuthally averaged.

(2) High-Resolution SAXS Experiment. We prepared a relatively thin film (<0.5 mm) by slicing a piece of sample with a razor blade and made a more finely collimated beam than in experiment 1.

(3) Rotation SAXS Experiment. We sliced a very thin piece of sample, ~0.1 mm thick, with a razor blade and inserted the

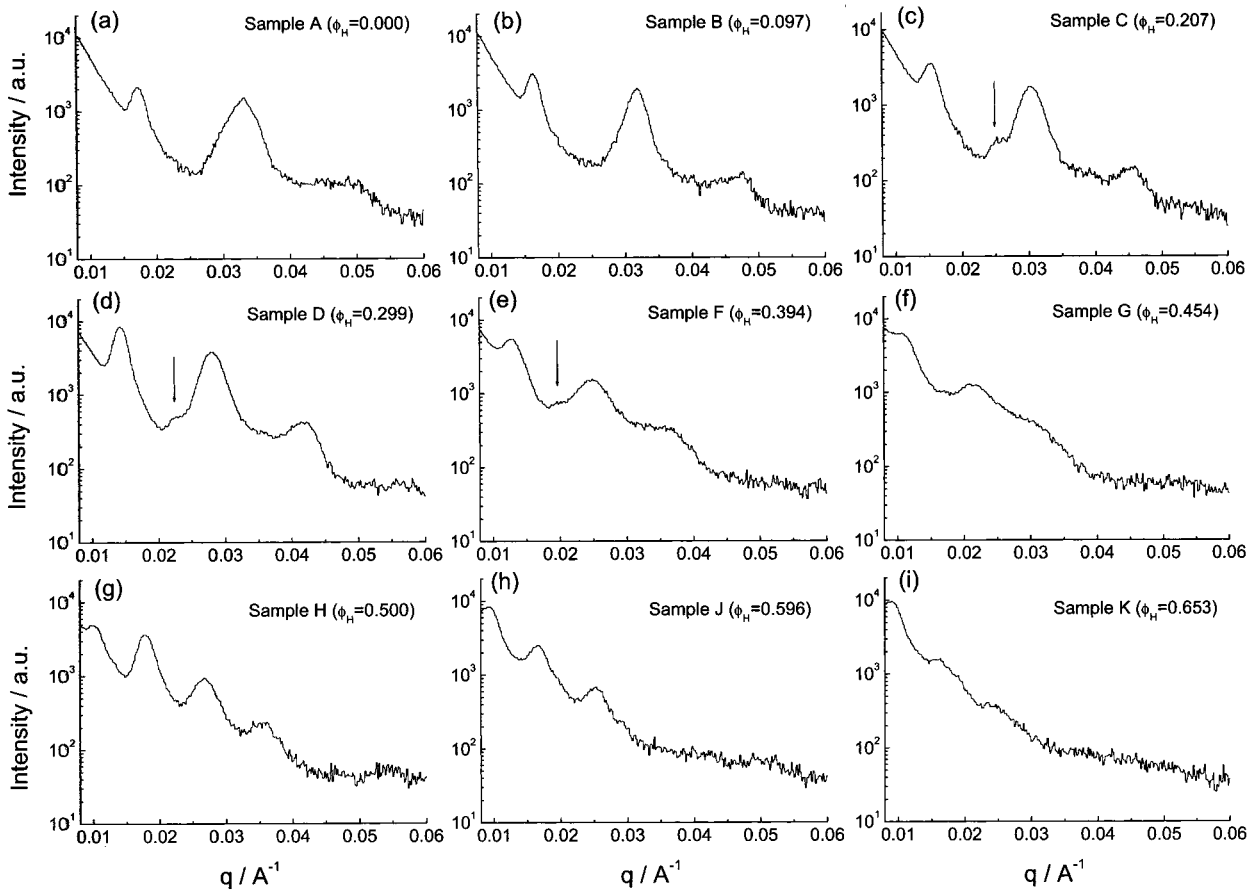

Figure 2. Dependence of SAXS profiles on total homopolymer volume fraction, ϕ_H: (a) sample A ($\phi_H = 0$, pure SID triblock copolymer), (b) sample B ($\phi_H = 0.097$), (c) sample C ($\phi_H = 0.207$), (d) sample D ($\phi_H = 0.299$), (e) sample F ($\phi_H = 0.394$), (f) sample G ($\phi_H = 0.454$), (g) sample H ($\phi_H = 0.500$), (h) sample J ($\phi_H = 0.596$), and (i) sample K ($\phi_H = 0.653$). SAXS profiles of sample E ($\phi_H = 0.352$) and sample I ($\phi_H = 0.546$) are similar to those of samples D and H, respectively. Inset arrows in c−e indicate the positions where the weak peak appears in region IB.

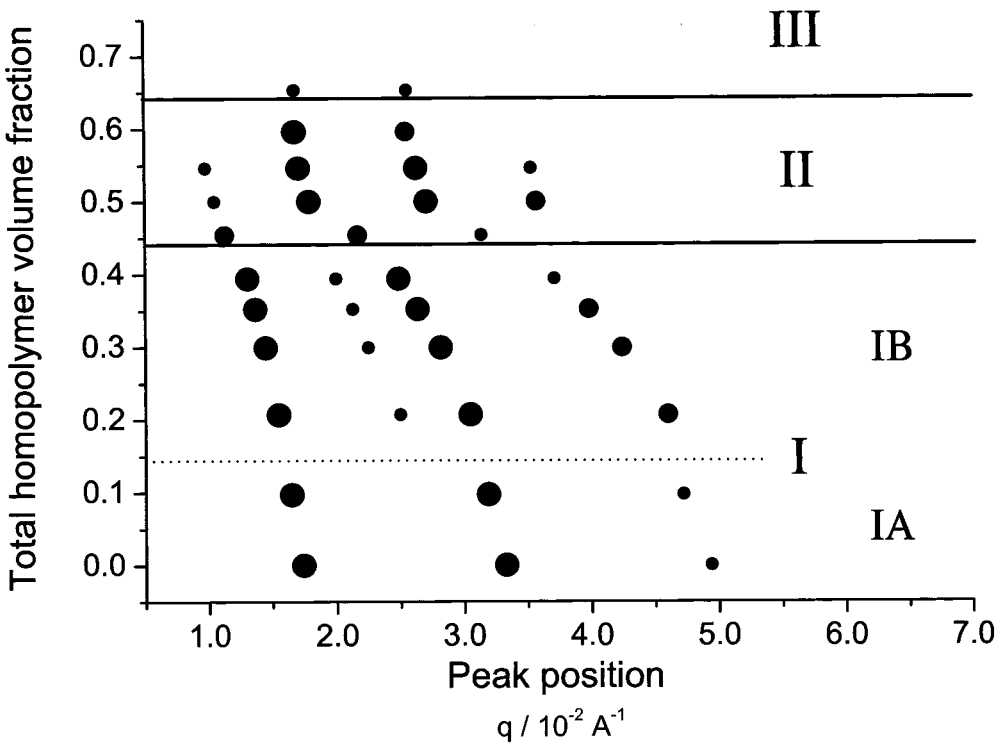

Figure 3. SAXS peak positions as a function of total homopolymer volume fraction. The size of a dot roughly indicates the intensity of the peak. Two solid lines and a broken line indicate the boundaries where the SAXS pattern changes. The upper solid line at $\phi_H \approx 0.65$ and the lower solid line at $\phi_H \approx 0.45$ indicate the boundaries between regions III and II and between regions II and I, respectively. The broken line indicates the boundary where region I could be divided into two regions, region IA and region IB.

slice into a capillary and rotated the capillary around one axis while irradiating with X-rays.

D. Small Angle Neutron Scattering. SANS experiments were conducted at the National Institute of Standards and Technology (NIST), Gaitherburg, MD. The neutron wavelength was $\lambda = 6.0$ Å with a spread of $\Delta\lambda/\lambda = 0.1$. An area detector was located 15 m from the sample yielding a q range of 5.0×10^{-3} to 5.0×10^{-2} Å^{-1}.

E. Transmission Electron Microscopy. TEM analysis was performed with a JEOL 1210 TEM operating at 120 kV. Ultrathin sections of the samples were obtained with a Reichert ultramicrotome equipped with a diamond knife. Slices 700 Å thick were cut at −120 °C to minimize deformation of the rubbery poly(dimethylsiloxane) and polyisoprene domains. Some sliced samples were stained with the vapor from a 4% aqueous solution of OsO_4 for 10 min. The contrast between polyisoprene and two other polymers increased in these samples because polyisoprene is selectively stained by OsO_4. Unstained samples have natural contrast between poly(dimethylsiloxane) and the two other polymers domains because of the higher electron density of silicon.

Results and Analysis

We begin the evaluation of the SAXS experiments performed on specimens listed in Table 1 by considering the number of different phases appearing over the range of total homopolymer volume fraction. Figure 2 shows several typical scattering profiles from SAXS experiment 1. Peaks of varying resolution and intensity are apparent in the scattering profiles of samples A−J for $\phi_H = 0.000-0.653$, indicating that, over this range, the blends have ordered structures. In addition, the scattering patterns from all samples are isotropic, with coaxial rings signifying that the samples consist of randomly oriented domains.

As shown in Figure 2, the scattering profiles change drastically at certain total homopolymer volume fractions. Adding the homopolymers to pure SID triblock copolymer (sample A) shifts the peak positions to lower q range but maintains their relative positions. When the total homopolymer volume fraction reaches 0.454 (sample G), the peaks become broad. At $\phi_H = 0.500$ (sample H), the peaks regain sharpness, but their positions relative to each other have changed completely. As more homopolymer is added, the peak positions shift to lower q range again until $\phi_H = 0.653$ (sample K) at which point all peaks have nearly disappeared. The shifts of the peak positions to lower q range mean that the dimension of the structure is expanding, and the changes in relative peak positions indicate changes in the morphology.

These changes are summarized in Figure 3, which maps the relationship between the peak positions and the total homopolymer volume fraction. Figure 3 is divided into three regions, each of which is associated with one morphology: region I occurs in the homopolymer volume fraction range between 0 and 0.45, region II between 0.45 and 0.65, and region III above 0.65 total homopolymer volume fraction. The boundaries are indicated with two solid lines in the figure. Region I might be further divided into two sections at $\phi_H \approx 0.15$, as suggested by the appearance of a weak peak, shown by inset arrows in Figure 2c−e. This boundary is indicated with a broken line in Figure 3. All observed peak positions and their relationships to the first peaks are indicated in Table 2.

A. Region III. When $\phi_H > 0.65$, the SAXS peaks apparent in the other regions have nearly disappeared, as shown in Figure 2i. Here, we employed TEM to elucidate the structure of sample K ($\phi_H = 0.653$) (see Figure 4.) A coarse heterogeneous morphology is evident, consistent with macroscopic phase separation. Considering the lower viscosities of the homopoly-

TABLE 2: Absolute and Relative SAXS Peak Positions

code	position ($Å^{-1}$) ratio[a]	position ($Å^{-1}$) ratio[a]	position ($Å^{-1}$) ratio[a]	position ($Å^{-1}$) ratio[a]
A	1.74×10^{-2} 1.00	– –	3.33×10^{-2} 1.91	4.94×10^{-2} 2.84
B	1.65×10^{-2} 1.00	– –	3.19×10^{-2} 1.93	4.72×10^{-2} 2.86
C	1.55×10^{-2} 1.00	2.50×10^{-2} 1.61	3.05×10^{-2} 1.97	4.60×10^{-2} 2.97
D	1.45×10^{-2} 1.00	2.25×10^{-2} 1.55	2.82×10^{-2} 1.94	4.24×10^{-2} 2.92
E	1.37×10^{-2} 1.00	2.13×10^{-2} 1.55	2.64×10^{-2} 1.94	3.98×10^{-2} 2.91
F	1.31×10^{-2} 1.00	2.00×10^{-2} 1.53	2.49×10^{-2} 1.90	3.71×10^{-2} 2.83
G	1.13×10^{-2} 1.00	– –	2.17×10^{-2} 1.92	3.14×10^{-2} 2.78
H	1.00×10^{-2} 1.00	1.79×10^{-2} 1.79	2.71×10^{-2} 2.71	3.57×10^{-2} 3.57
I	0.98×10^{-2} 1.00	1.71×10^{-2} 1.74	2.63×10^{-2} 2.68	3.53×10^{-2} 3.60
J	– –	1.68×10^{-2} 1.00	2.55×10^{-2} 1.52	– –
K	– –	1.68×10^{-2} 1.00	2.56×10^{-2} 1.52	– –

[a] Ratio is the value of the peak position divided by the first peak position.

mers relative to the triblock copolymer, the light regions likely correspond to homopolymer-rich regions where the polymers fell from the sample during or after microtoming; the darker, nanostructured regions most likely correspond to homopolymer-poor sections. In the dark regions, an ordered structure is seen, which is highlighted in an inset in Figure 4. The very weak and broad peaks observed in Figure 2i could be attributed to this local ordered structure. As shown in Figure 3, the peak positions of sample K ($\phi_H = 0.653$, region III) are almost the same as the peaks of of sample J ($\phi_H = 0.596$, region II), even though the peak intensities are different. Therefore, the local ordered structure in the homopolymer-poor regions is expected to be similar to the structure in region II. We shall return to the detailed structure in the homopolymer-poor regions after discussing the structure of region II.

B. Region II. *1. High-Resolution SAXS Experiment.* Type-2 SAXS experiments with sample H ($\phi_H = 0.500$) produced single-crystal-like diffraction patterns. A two-dimensional scattering pattern and its azimuthally averaged one-dimensional scattering profile are shown in Figure 5a and b, respectively. The peak positions and their ratios are listed in Table 3. In Figure 5b, the first peak at 9.86×10^{-3} $Å^{-1}$ is better resolved than that in Figure 2g, and the second peak of Figure 2g is resolved into two reflections at 1.71×10^{-2} and 2.00×10^{-2} $Å^{-1}$.

As indicated in Table 3, the relative peak positions agree well with a structure having two-dimensional hexagonal symmetry. In addition, the angular relationships between all spots shown

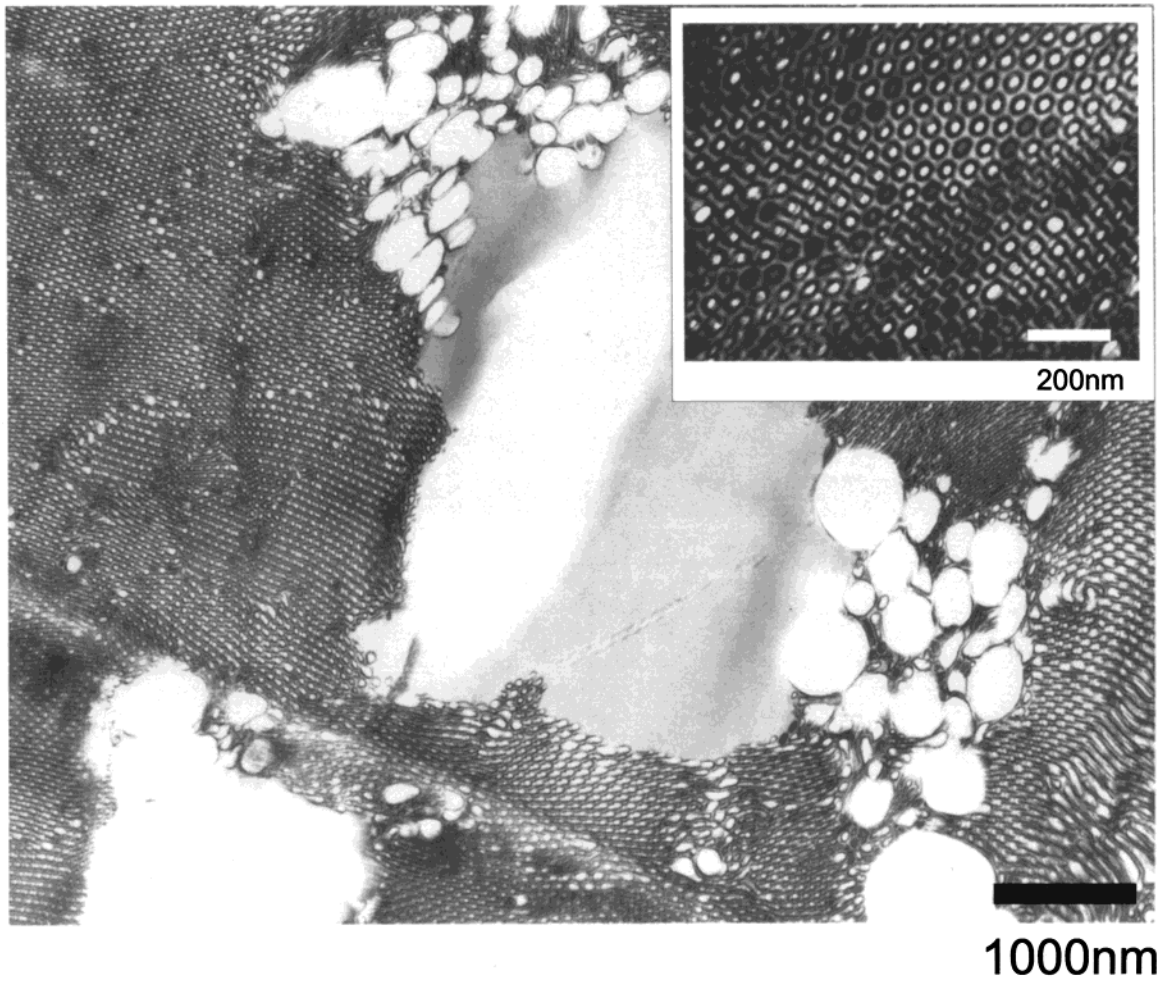

Figure 4. TEM image of sample K ($\phi_H = 0.653$, region III). This sample was stained with OsO_4. The dark and light regions correspond to the homopolymer-poor and -rich domains, respectively. The inset figure is an enlarged image of the dark region.

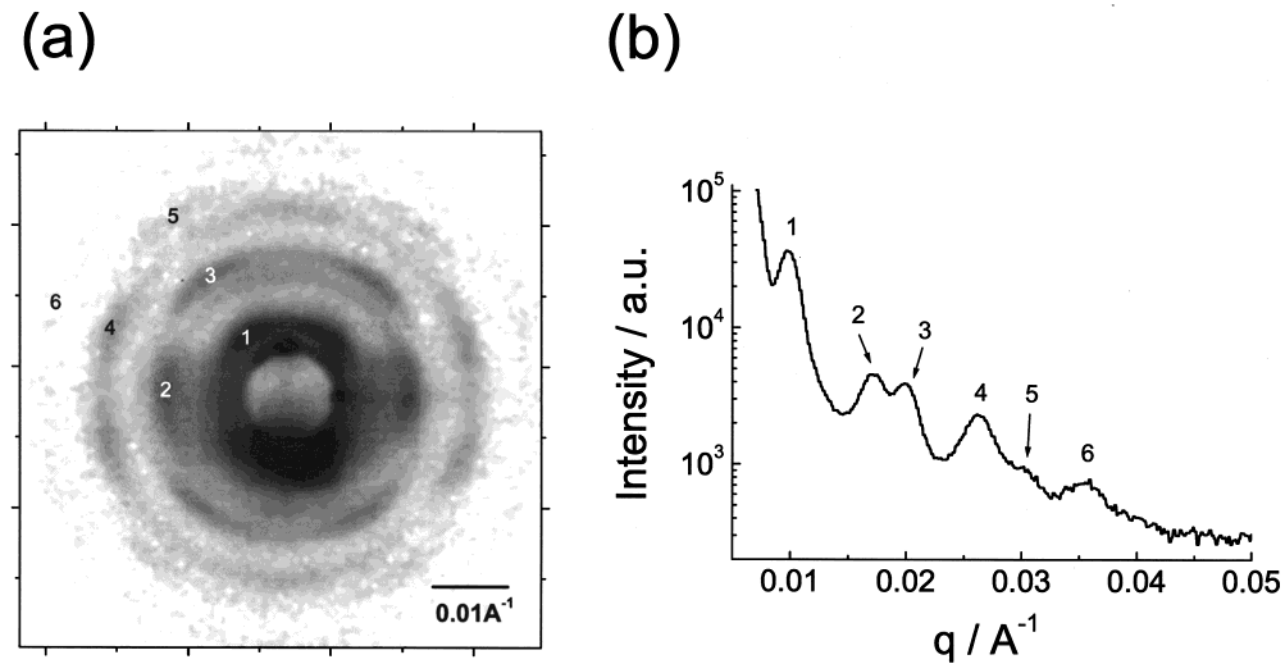

Figure 5. (a) Two-dimensional scattering pattern and (b) its one-dimensional profile from a thin film of sample H ($\phi_H = 0.500$, region II) by SAXS experiment 2. The inset numbers indicate the peak positions referred to in Table 3. The gray circular shadow in the center of panel a shows the beam stop, and the high-intensity region just below the beam stop is due to the parasitic scattering. Panel b shows how the second peak in Figure 2g can be resolved into two reflections.

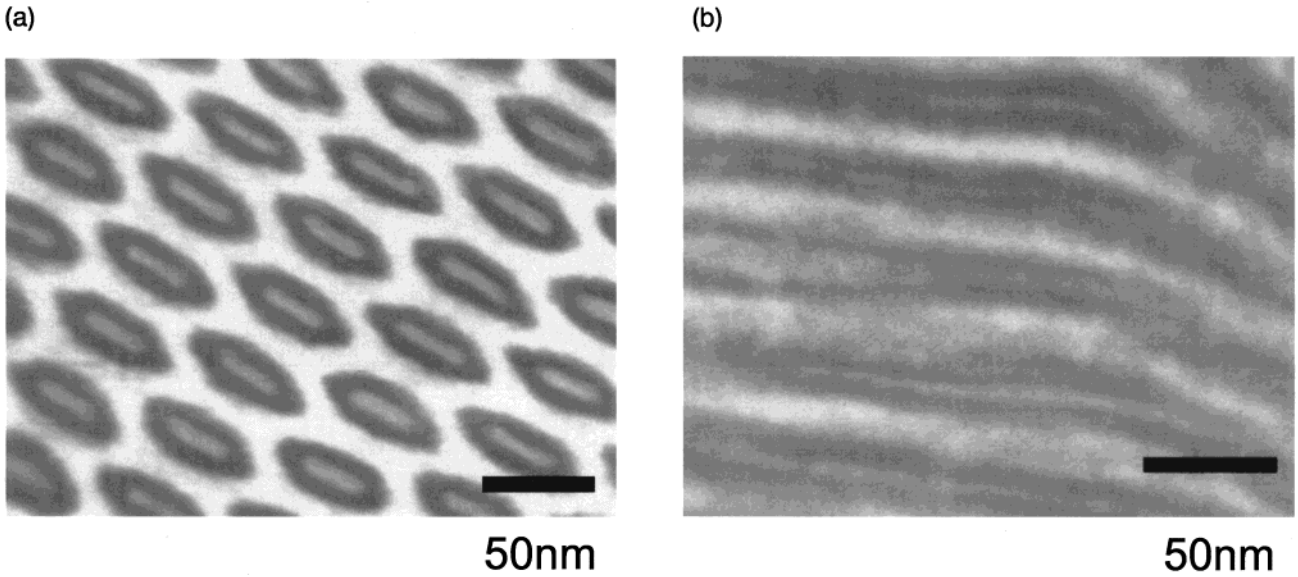

Figure 6. TEM images of sample I ($\phi_H = 0.546$, region II). This sample was stained with OsO_4. The white, black, and gray regions correspond to polystyrene, polyisoprene, and poly(dimethylsiloxane), respectively. (a) Cross sections of the core−shell tubes and their packing structure and (b) a side view of the core−shell tubes.

TABLE 3: SAXS Reflections from Sample H

observed			2D hexagonal	
no.	position (Å^{-1})	ratio	order	ratio
1	9.86×10^{-3}	1.00	1	1.00 (= $\sqrt{1}$)
2	1.71×10^{-2}	1.74	2	1.73 (= $\sqrt{3}$)
3	2.00×10^{-2}	2.03	3	2.00 (= $\sqrt{4}$)
4	2.62×10^{-2}	2.66	4	2.65 (= $\sqrt{7}$)
5	3.03×10^{-2}	3.07	5	3.00 (= $\sqrt{9}$)
–	–	–	6	3.46 (= $\sqrt{12}$)
6	3.55×10^{-2}	3.60	7	3.61 (= $\sqrt{13}$)

in Figure 5a agree with those expected for a two-dimensional hexagonal structure, assuming that the scattering plane is tilted by 52°.

2. TEM Analysis. We also performed TEM on a stained section of sample I ($\phi_H = 0.546$, region II) to aid in evaluating the morphology. In Figure 6a we see gray regions of PDMS surrounded by black domains of PI embedded in a white matrix of PS. Hexagonal symmetry, suggested by the SAXS results, is not immediately apparent from Figure 6a. This could result from slicing the cylinders at an angle that is not perpendicular to their axes or from deformation of the material during microtoming. In a TEM image corrected for tilt by simple geometry, the *d* spacing is approximately 60 nm. From the first peak in SAXS, the *d* spacing is 63 nm. These numbers are within the experimental error of the TEM as measured from calibrated gratings. In addition, the tubes of this structure have nonconstant mean curvature with well-defined corners. Figure 6b is a layered

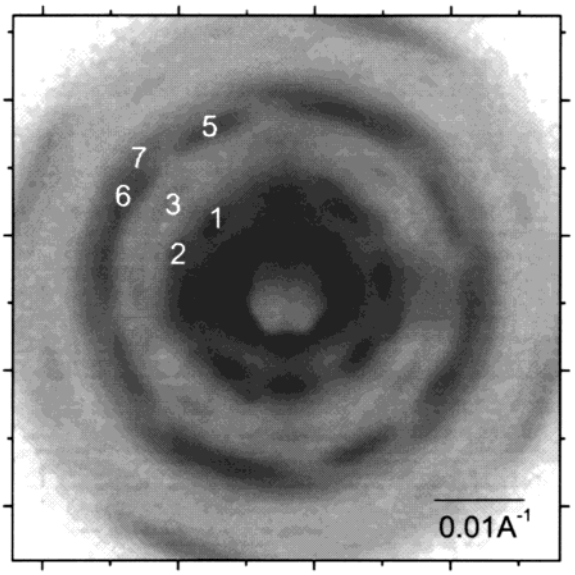

Figure 7. Two-dimensional scattering pattern from a thin film of sample D ($\phi_H = 0.299$, region IB) by SAXS experiment 2. The numbers indicate the peak positions referred to in Table 4.

TABLE 4: Two-Dimensional SAXS Reflections from Sample I

observed			*Ia*$\bar{3}$*d*		
no.	position (Å^{-1})	ratio	order	index	ratio
1	1.44×10^{-2}	1.00	1	211	1.00 (= $\sqrt{6/6}$)
2	1.65×10^{-2}	1.15	2	220	1.15 (= $\sqrt{8/6}$)
3	2.21×10^{-2}	1.53	3	321	1.53 (= $\sqrt{14/6}$)
(4)[a]	(2.35×10^{-2})[a]	(1.63)[a]	4	400	1.63 (= $\sqrt{16/6}$)
5	2.65×10^{-2}	1.84	5	420	1.83 (= $\sqrt{20/6}$)
6	2.75×10^{-2}	1.91	6	332	1.91 (= $\sqrt{22/6}$)
7	2.97×10^{-2}	2.04	7	422	2.00 (= $\sqrt{24/6}$)

[a] This scattering spot is observed from another sample D.

image, consistent with a projection of a tubular morphology normal to the axis of the tubes. From the TEM results, it is clear that the morphology is coaxial tubes consisting of PDMS cores and PI shells in a PS matrix, and from the SAXS results, we can conclude that these tubes are hexagonally packed.

Now we return to the ordered structure in region III. Because the sample was stained with OsO_4, the white, black, and gray regions in Figure 4 correspond to polystyrene, polyisoprene, and poly(dimethylsiloxane) domains, respectively. In the inset of Figure 4, hexagonally packed coaxial tubes of poly(dimethylsiloxane) cores (gray) surrounded by polyisoprene shells (black) in a matrix of polystyrene (white), are apparent in the homopolymer-poor sections similar to those seen in Figure 6a. (The centers of some tubes are white, which we attribute to the removal of the low-molecular-weight PDMS during or after microtoming.) This is consistent with the result that the peak positions of sample K ($\phi_H = 0.653$, region III) are almost same as those of sample J ($\phi_H = 0.596$, region II). Therefore, we believe that the morphology of the homopolymer-poor regions in region III is the core−shell cylindrical structure.

C. Region IB. *1. High-Resolution SAXS Experiment.* SAXS protocol 2, applied to a thin specimen of sample D ($\phi_H = 0.299$), yielded SAXS spot patterns, one of which is shown in Figure 7. This diffraction pattern reveals that the first three peaks in Figure 2c are actually composed of six reflections. As indicated in Table 4, the relative peak positions are in good agreement with those allowed by the *Ia*$\bar{3}$*d* space group, with the exception of the ⟨400⟩ reflections, which are not evident. However, we

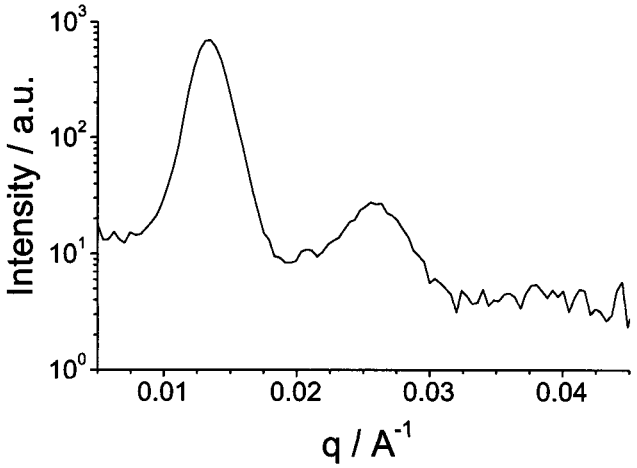

Figure 8. SANS profile of sample D ($\phi_H = 0.299$, region IB). Lack of a reflection at $q < 0.01$ Å^{-1} is consistent with a core−shell gyroid morphology.

did record diffraction spots in SAXS patterns obtained from another piece of sample D that were consistent with a ⟨400⟩ assignment.

2. SANS Experiment. To substantiate that the reflection at 1.44×10^{-2} Å^{-1} in sample D is the lowest order of diffraction, we employed SANS, which accesses low scattering vectors and a different set of scattering contrast factors. Figure 8 shows the scattering profile between 5.0×10^{-3} and 4.5×10^{-2} Å^{-1}. Within the attainable signal-to-noise and q resolution the first diffraction peak appears at 1.4×10^{-2} Å^{-1}, consistent with SAXS data. If the sample had *I*4$_1$32 symmetry, which is the space group of the alternating gyroid,[19] there should be ⟨110⟩ reflections at 8.32×10^{-3} Å^{-1}. Thus, we can reduce our analysis to *Ia*$\bar{3}$*d* and *I*$\bar{4}$3*d* as the most likely candidate symmetries. (However, accidental contrast matching, as occurred in the ISD core−shell gyroid,[8] could account for the absence of a low-q peak, although not simultaneously in SAXS.)

3. Rotation SAXS Experiment. Upon closer examination of the pattern in Figure 7, we see that the sample is not completely single-crystal-like because there are eight spots at 1.44×10^{-2} Å^{-1} when there should be maximum six ⟨211⟩ reflections in one scattering plane. To examine the angular relationships between scattering spots in a single-crystal-like sample, we prepared a thinner sample (∼0.1 mm) and performed the SAXS experiments described in protocol 3. Figure 9a shows the spot pattern at an initial position, and Figure 9b shows the scattering pattern obtained from the sample rotated by 30° from the initial position. The two scattering patterns are significantly different, implying that they correspond to different scattering planes and that the sample is a "single crystal".

The angular relationships between ⟨211⟩ reflections in a cubic unit cell can have one of five fixed values, 33.6°, 48.2°, 60.0°, 70.6°, and 80.4°. All angular relationships between the scattering spots recorded at 1.44×10^{-2} Å^{-1} by experiment 3 match one of these five allowed angles. Furthermore, all scattering spots in Figure 9a and b have been indexed from their angular relationships and the rotational angle between the scattering planes. With this result, we deduce that the scattering planes of Figure 9a and b are ($3\bar{5}1$) and ($1\bar{1}1$), respectively.

The space groups *I*$\bar{4}$3*d* and *Ia*$\bar{3}$*d* both have ⟨211⟩ and ⟨220⟩ reflections as the first and second allowed reflections.[28] In the *I*$\bar{4}$3*d* space group sets of ⟨$\bar{1}$03⟩ and ⟨10$\bar{3}$⟩ reflections should appear at $|q| = 1.86 \times 10^{-2}$ Å^{-1} in Figure 9a. Although only the appearance of reflections can conclusively determine the symmetry of a sample, the absence of the ⟨$\bar{1}$03⟩ and ⟨10$\bar{3}$⟩

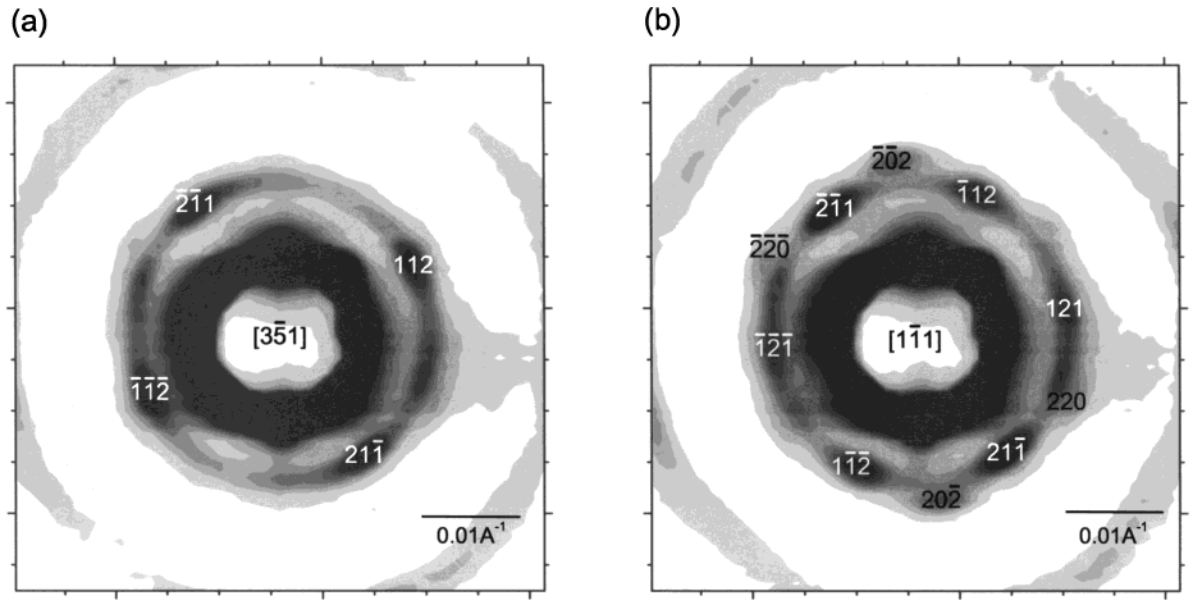

Figure 9. Two-dimensional SAXS patterns obtained from rotational SAXS experiment (protocol 3). (a) This pattern is consistent with the X-ray beam incident on the (3$\bar{5}$1) plane with *Ia*$\bar{3}$*d* symmetry. The scattering spots are indexed as the single-crystal belonging to *Ia*$\bar{3}$*d*. (b) This pattern was obtained after rotating from the sample (a) by 30°. This set of the reflections is consistent with a scattering plane of (111) with *Ia*3*d* symmetry. The scattering spots are also indexed as the single-crystal belonging to *Ia*$\bar{3}$*d*.

reflections nevertheless suggests that the *Ia*$\bar{3}$*d* space group is the proper assignment for region IB.

4. TEM Analysis. We turned to TEM to further elucidate the morphology of the structure with tentative *Ia*$\bar{3}$*d* symmetry. Microtoming uniform and mechanically sound thin slices from specimens in region IB was difficult, resulting in relatively poor TEM images. In Figure 10a, which is the TEM image of an unstained slice of sample D, the dark regions correspond to poly(dimethylsiloxane), and the white regions to polystyrene and polyisoprene. Figure 10a has dark spots connected by four arms and shows *c*2*mm* plane symmetry. This figure is very similar to the TEM image of the projection along the [110] direction of a gyroid structure observed in an ABA triblock copolymer.[29,30] Assuming this morphology and accepting the same projection, the distance between connected poly(dimethylsiloxane) spots, *d*, is given by

$$d = \sqrt{\frac{3}{2}}\frac{a}{4} \qquad (1)$$

where *a* is the cubic lattice parameter. From Figure 10a, *d* was measured along the direction marked and was found to be 300 ± 30 Å, and the first-order scattering was calculated to be (1.1 ± 0.2) × 10^{-2} Å^{-1}. This value agrees with that determined by SAXS and SANS, 1.44 × 10^{-2} Å^{-1}. To confirm that the image in Figure 10a is consistent with the [110] projection of the gyroid morphology, we used TEMSIM,[31] a software program that generates projections of different morphologies, which are constructed from level surfaces, along specified crystallographic directions. In Figure 10c, the projection along the [110] direction of a gyroid morphology having networks of PDMS occupying 30 vol % of the structure is shown. The agreement with Figure 10a is good.

Figure 10b is a TEM image of a stained sample. In a complicated morphology, it is difficult to distinguish the gray region (PDMS) from the black region (PI) because of a convolution of mass thickness contrast. To interpret the image in Figure 10b, we used TEMSIM to generate a core−shell gyroid morphology with cores of D, shells of I, and a matrix of S, which had volume fractions 0.3/0.4/0.3 of the three polymeric species S/I/D, respectively, as in sample D. The [111] projection of this model, shown in Figure 10d, captures the distinctive features of Figure 10b, indicating that the structure is consistent with a core−shell gyroid morphology.

D. Region IA. *1. SAXS and SANS Experiments.* As shown in Figure 2a, the peak positions between the first, second, and third peaks in the SAXS profile of the neat SID triblock copolymer were 1.72 × 10^{-2}, 3.29 × 10^{-2}, and 4.73 × 10^{-2} Å^{-1}, respectively. Their relationships are 1:1.91:2.76, indicating the structure is not lamellar. The SANS profile of the neat SID triblock (not shown) also has the first peak at 1.71 × 10^{-2} Å^{-1}. Therefore, we assumed that the peak at 1.72 × 10^{-2} Å^{-1} is the first reflection and that the distance between the corresponding planes is around 370 Å. The second peak at 3.29 × 10^{-2} Å^{-1} is relatively broad, implying that it consists of several peaks.

Here, we expect a spot pattern to reveal the structure in detail, as seen in the previous sections. Therefore, sample A was dynamically sheared (100% shear strain amplitude at 1-Hz frequency and 200 °C) to induce long-range order and then used in type-2 SAXS experiments. Figure 11 shows one of the recorded spot patterns, and Table 5 lists the *q* values for the first 10 spots and their relative positions. The numbers on the spots in Figure 11 indicate those in the table. Comparing the scattering positions obtained from the sheared neat SID triblock (indicated in Table 5) with those from the unperturbed material, we note two differences: (i) the first peak from the sheared sample is shifted to a higher *q* region, and (ii) five distinct SAXS reflections from the sheared sample (2−6 in Table 5) replace the broad second peak characterizing the undistorted sample. The shift in the location of the first peak is attributed to the difference in the annealing temperatures, 150 and 200 °C with and without shear, respectively.

2. TEM Analysis. Figure 12 shows TEM images from slices of the neat SID triblock; 12a and b are from the unstained specimens, while 12c and d are from the stained materials. None of these images is consistent with the familiar projections of the gyroid or core−shell gyroid morphologies. In Figure 12a,

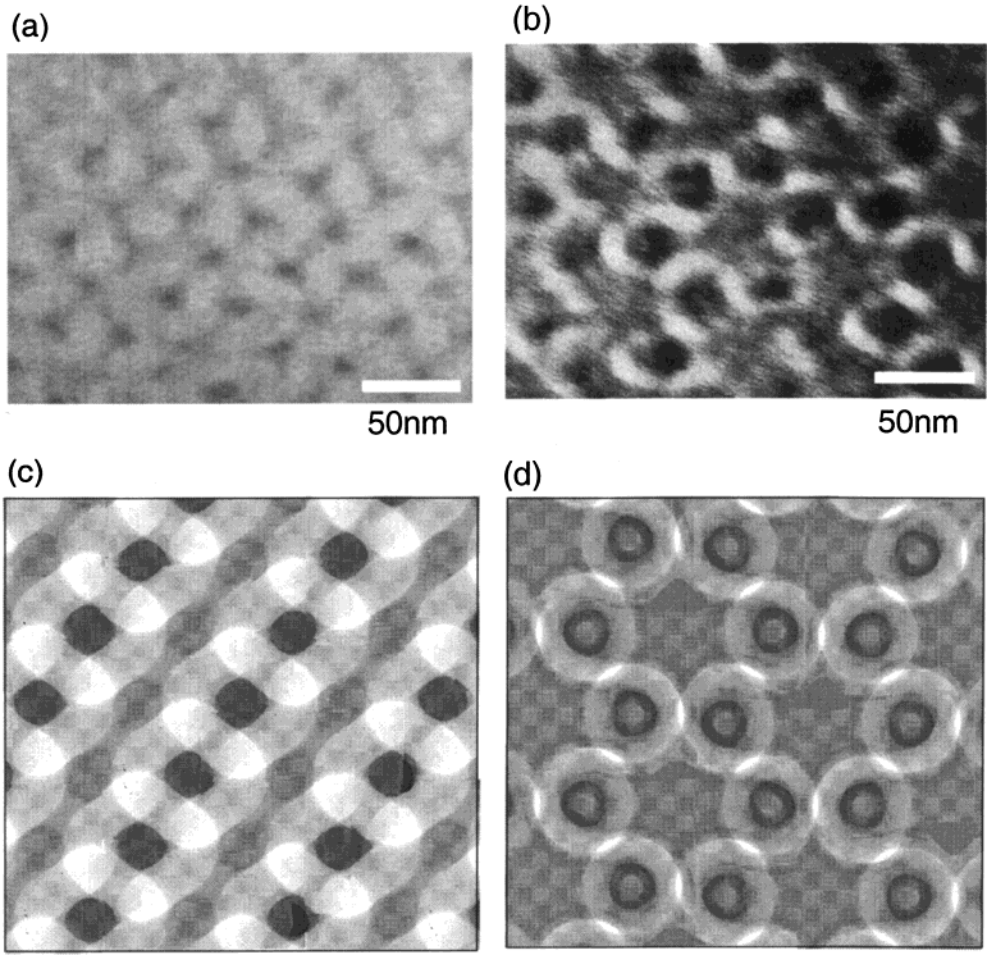

Figure 10. TEM images of sample D ($\phi_H = 0.299$, region IB) for (a) unstained and (b) stained specimens. (c) Projection along [110] of a gyroid constructed in TEMSIM with level surfaces with 30 vol % PDMS. (d) Projection along [111] direction of a core−shell gyroid generated by four level surfaces in TEMSIM to have 30 vol % gray cores, 40 vol % black shells, and 30 vol % white matrix.

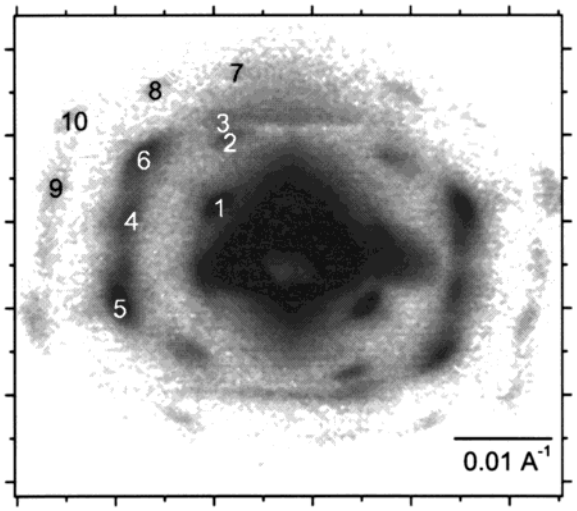

Figure 11. Two-dimensional SAXS pattern obtained from a sheared sample of neat SID triblock copolymer. The numbers indicate the first 10 peak positions (see text).

gray circles are tetragonally arranged in a white matrix, and in Figure 12b, alternating white and gray layers are apparent. Because the gray corresponds to poly(dimethylsiloxane) (D) domains in the unstained image, the gray projections shown in Figure 12a and b are consistent with tetragonally packing of D cylinders. From Figure 12a, the distance between the nearest two D cylinders is found to be around 260 Å.

TABLE 5: Observed First 10 Reflections from Sheared SID

no.	position (Å^{-1})	ratio	index (FCC)	ratio
1	1.92×10^{-2}	1.00	111	1.00
2	3.06×10^{-2}	1.59	–	–
3	3.23×10^{-2}	1.68	220	1.63
4	3.48×10^{-2}	1.81	–	–
5	3.67×10^{-2}	1.91	311	1.91
6	3.82×10^{-2}	1.99	222	2.00
7	4.42×10^{-2}	2.30	400	2.30
8	4.79×10^{-2}	2.49	331	2.51
9	5.07×10^{-2}	2.64	420	2.58
10	5.50×10^{-2}	2.86	422	2.83

We turn to the stained images, Figure 12c and d, assuming that the D domains are tetragonally packed cylinders. In Figure 12c, white circles corresponding to polystyrene (S) domains show very nearly 4-fold symmetry. In addition, a smaller gray circle appears nested in the center of the four white circles (S domains) also with 4-fold symmetry. Because the distance between the nearest two gray circles is measured to be around 270 Å and is very similar to the distance between the nearest two D cylinders in Figure 12a, it is rational to conclude that the gray circle corresponds to an end-on projection of the D cylinder. In Figure 12d, the white circles show a different arrangement, and gray lines run through the white circles. These gray lines of D domains imply that Figure 12d is a projection onto a plane perpendicular to the plane of Figure 12c (or a). Therefore, the S domain must be spherical as it produces a white circle in both Figure 12c and d. In addition, the arrangement of

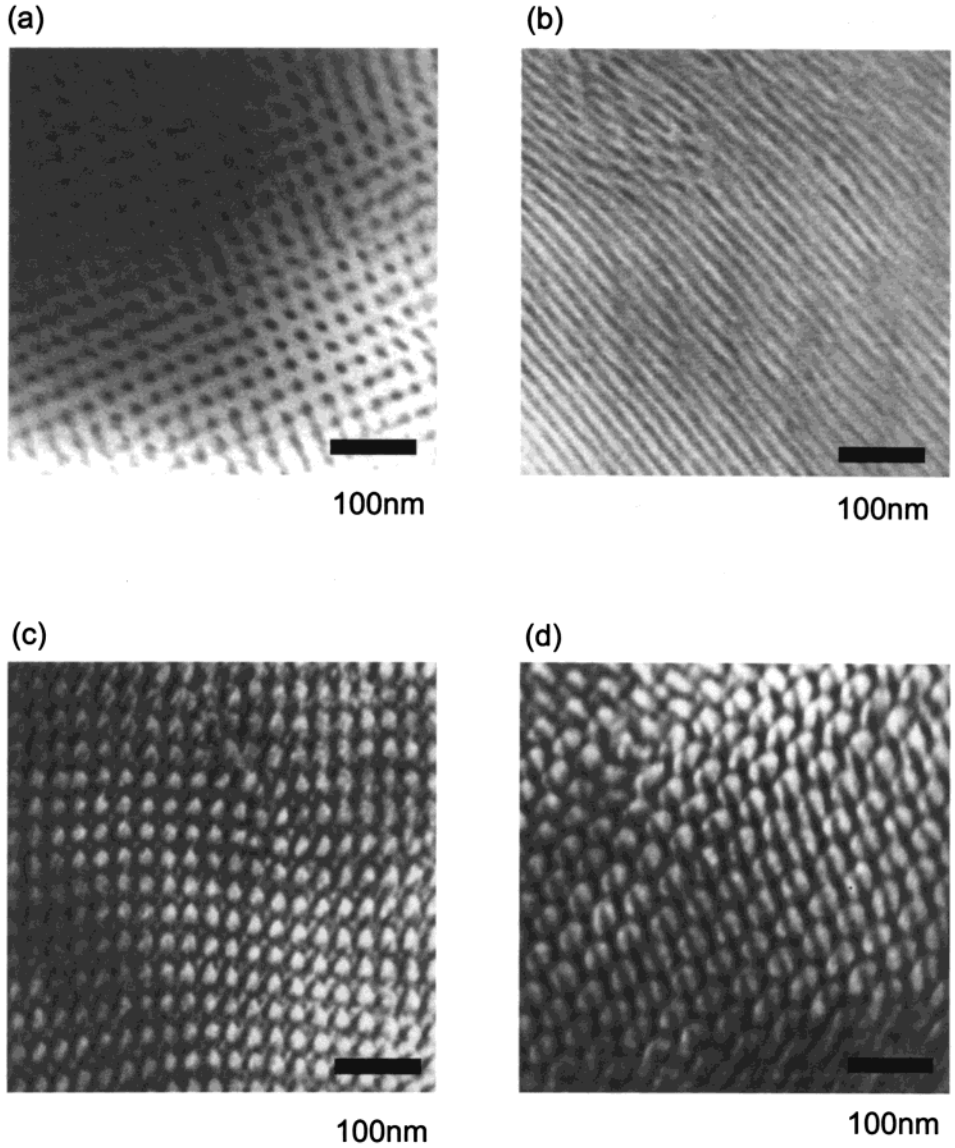

Figure 12. TEM images of the neat SID triblock copolymer. Images of the unstained sample, (a) and (b), show gray regions corresponding to PDMS domains. The white regions correspond to PI and PS domains. The stained sample produces images with white, gray, and black regions, (c) and (d), corresponding to PS, PDMS, and PI domains, respectively. In panel a, the gray circles exhibit 4-fold symmetry and the distance between the nearest circles is 270 Å. In panel c, the white circles show very nearly 4-fold symmetry, and a smaller gray circle appears in the center of the four white circles with 4-fold symmetry. The distance between the nearest two gray circles is 280 Å.

the white circles in Figure 12d means that the nearest two S spheres in Figure 12c reside in different planes. Furthermore, considering the χ-parameter relationship, $\chi_{SI} = 0.06$,[23] $\chi_{ID} = 0.09$,[24] and $\chi_{SD} = 0.20$[24] at 150 °C, the gray lines running through the white circles are probably not D domains surrounded by S, but rather arise from a projection of the D domains onto the S domains. In other words, the S sphere is surrounded by the four D cylinders in an I matrix.

On the basis of these observations, we deduce four features for the morphology of the neat SID: (i) the S domains are spherical; (ii) the D domains are tetragonally packed cylinders; (iii) the S spheres are surrounded by the tetragonally packed D cylinders; and (iv) adjacent S spheres with apparent 4-fold symmetry, obtained by projections along the long axis of D cylinders, lie on different planes.

3. Possible Candidate for Morphology of Neat SID. Judging from the TEM images, we suggest the morphology illustrated in Figure 13a−c as that of the neat SID: Figure 13a and b corresponds to Figure 12c (or a) and d, respectively. The white and light gray shadings signify two levels of S spheres, and the dark gray denotes the D cylinders. The unit cell is a tetragonal lattice with $a = c = 2b = 370$ Å, indicated with thin squares. However, we adopt a cubic cell with $a = 740$ Å, identified with thick squares. The cubic cell consists of nine white S spheres at $z = 0$ (and/or $z = 1$) and four light gray S spheres at $z = {}^1/_2$, and the D cylinders run through four equivalent sites, $(x,y) = ({}^1/_4, {}^1/_4)$, $({}^1/_4, {}^3/_4)$, $({}^3/_4, {}^1/_4)$, and $({}^3/_4, {}^3/_4)$. In Figure 13a, $d_1(\{220\})$ and $d_2(\{040\} = \{400\})$ are the first and second longest periodic distances, 260 and 185 Å ($= d_1/\sqrt{2}$), respectively. The corresponding scattering reflections appear at 0.024 and 0.034 Å^{-1}, respectively. In Figure 13b, the longest periodic distance d_3 is 370 Å, and the corresponding scattering peak should appear at 0.017 Å^{-1}, which was the observed first peak at 0.0172 Å^{-1}. Other allowed reflections are listed in Table 6.

Now, we compare our suggested morphology with the SAXS results from the sheared sample. [Note that the unperturbed SAXS pattern (Figure 2) has insufficient detail to warrant such evaluation.] A comparison of the calculated reflections (Table 6) with the recorded ones for the sheared sample (Table 5) reveals a serious inconsistency. We believe that this disparity

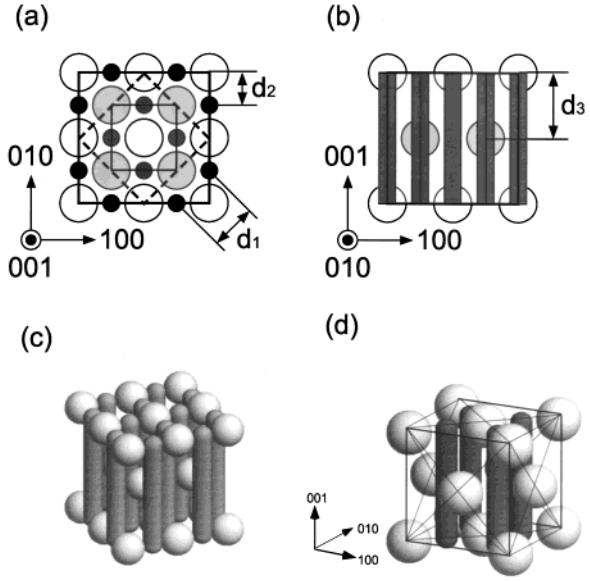

Figure 13. Illustration of the morphology of neat SID triblock copolymer. (a) The projections along the 001 direction of the morphology of the neat unperturbed SID triblock copolymer. White and light gray circles indicate S domains, and dark gray circles indicate D domains. White and gray circles do not reside in same plane. (b) The projections along 010 direction of the morphology of the unperturbed SID triblock copolymer. White and light gray circles indicate S domains, and dark gray rectangles indicate D domains. (c) Perspective view of the morphology of the unperturbed SID triblock copolymer. Spheres and cylinder show S and D domains, respectively. (d) Perspective view of the morphology of the sheared SID triblock copolymer. The spheres (S) form an FCC lattice, whereas the cylinders represent D domains.

TABLE 6: Anticipated Reflections for the Tentative Morphology of the Neat SID

no.	index	ratio	position ($Å^{-1}$)
1	002	1.00	1.72×10^{-2}
2	201	1.12	1.92×10^{-2}
3	220	1.41	2.43×10^{-2}
4	222	1.73	2.98×10^{-2}
5	203	1.80	3.10×10^{-2}
6	400	2.00	3.44×10^{-2}
7	421	2.29	3.94×10^{-2}
8	205	2.69	4.63×10^{-2}
9	440	2.83	4.86×10^{-2}
10	006	3.00	5.16×10^{-2}

was induced by a slight change in the lattice parameters during shearing. Specifically, along the 110 direction, the cell lengthens, and the unit cell changes to FCC as shown in Figure 13a by the dashed square. This modification is shown in Figure 13d. For the FCC structure, the first observed (110) reflection appears at 0.0192 $Å^{-1}$, which corresponds to the (201) reflection in the previous cubic cell. Therefore, these two reflections have similar q values. Assuming the FCC lattice, the 3 and 5−10 reflections can be assigned as the ⟨220⟩, ⟨311⟩, ⟨222⟩, ⟨400⟩, ⟨331⟩, ⟨420⟩, and ⟨422⟩ reflections, respectively, as indicated in the right two columns of Table 5. Two reflections, 2 and 4, cannot be assigned. We have no definitive explanation for this shortcoming. However, a reasonable explanation would be that they derive from residual unsheared polymer. We conclude that the morphologies depicted in Figure 13 are plausible but not definitive. A more precise analysis and experiments for the neat SID triblock copolymer are in progress.

Discussion

Figure 14 summarizes the progression of phases identified in the nearly symmetric SID/S/D system. (We cannot conclusively identify the morphology of the neat SID triblock at this point.) The addition of a small amount of PS and PDMS homopolymers, in volumes equal to that of the triblock, creates a core−shell gyroid structure in a remarkably wide range of ϕ_H, $\Delta\phi_H \approx 0.3$. As more homopolymer is added, the morphology changes to hexagonally packed core−shell tubes before phase separation at approximately 65 vol % homopolymer.

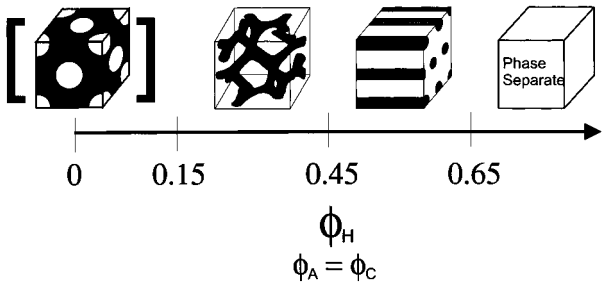

Figure 14. Progression of morphologies as equal amounts of PDMS and PI homopolymers are added to SID triblock copolymer. The morphology of neat SID has not been conclusively determined.

We attribute the appearance and persistence of core−shell structures, as well as the occurrence of phase separation (as opposed to microemulsion formation),[14] in this system to the small asymmetry in the χ parameters ($\chi_{SI} < \chi_{ID}$). This effect is most easily understood in the core−shell tube morphology (see Figure 6). A D core is surrounded by an I shell and embedded in an S matrix, resulting in a smaller ID interfacial area, relative to that for SI, consistent with the asymmetric χ parameters ($\chi_{SI} = 0.06$[23] and $\chi_{ID} = 0.09$[24]). In a blend of SID triblock with S and D homopolymers, we expect to find more S homopolymer in the corona of the S block than D homopolymer in the corona of the D block because the penalty for contact between the I block and D homopolymer is larger, as indicated by these χ parameters. This distribution of homopolymer further favors the expanded SI interface expected from asymmetric χ parameters. Thus, small asymmetries in χ in ABC/A/C blends affect not only the interfacial area between the blocks but also the distribution of homopolymer within the end blocks, making the core−shell morphologies, gyroid and cylinder, more prevalent than the alternating structures observed in other systems.[18,19] In the limit where a tricontinuous microemulsion is anticipated,[14] this delicate imbalance apparently leads to macroscopic phase separation.

The TEM images of the core−shell tube structures in region II have two key differences from projections of hexagonally packed core−shell cylinders. First, the gray cores appeared to be oblong, probably because of an oblique projection of the tube axis. The second distinguishing characteristic is the facetted interfaces between the core and shell and between the shell and matrix. In a projection parallel to the axis of the tube, these facets could arise from a tube with a hexagonal cross section. Such hexagonal cross sections have been observed in a neat poly(2-vinylpyridine-*b*-isoprene-*b*-styrene) (VIS) triblock copolymer with cores of poly(2-vinylpyridine), shells of polyisoprene, and a matrix of polystyrene.[32] When a small amount of low-molecular-weight polystyrene homopolymer was added, the structure maintained its hexagonal cross section.[33] However, when a high-molecular-weight homopolymer was added to the matrix, the structure had a circular cross section. These results suggest that the neat triblock and its blend with low-molecular-weight polystyrene homopolymer are frustrated in that they cannot simultaneously fill space uniformly and maintain interfaces with constant mean curvature. The high-molecular-weight homopolymer segregates to the corners of the Wigner−Seitz

cell, allowing the blocks near the corners of the cell to relax from their stretched configuration and form a matrix−shell interface with uniform mean curvature. As discussed above, in our SID/S/D system, the low-molecular-weight homopolymer is most likely distributed throughout the S domain and not segregated to the corners of the Wigner−Seitz cell, where it would relieve packing frustration but not aid in stabilizing the SI interface. Thus, strictly speaking, the structure consists of hexagonally packed core−shell tubes with hexagonal interfaces.

Tricontinuous morphologies, such as the core−shell gyroid structure found in the SID/S/D system presented here, might be important in future applications of block copolymers such as membranes. The isotropic character of these structures eliminates the need to align the microdomains with the direction of interest in applications that rely on transport through the material. The blending approach taken here facilitates the formation of tricontinuous phases while eliminating the tedious synthesis of block copolymers of different compositions. We also have four co-continuous microphase-separated structures in blends of an ABC triblock copolymer with the corresponding B homopolymer, for example, by swelling the middle block.[34] Preliminary evidence suggests that this blending approach is more sensitive to the amount of added homopolymer.

Tricontinuous polymeric microemulsions have been suggested as attractive co-continuous materials for engineering applications. We believe that these structures do not form in the SID system for three reasons. First, the slight asymmetry in the χ parameters drives the blends to form core−shell structures. This thermodynamic asymmetry might be countered by blending homopolymers of unequal molecular weights. For example, blending a higher-molecular-weight polystyrene homopolymer would increase the level of segregation between the S homopolymer and the polyisoprene block, counterbalancing the less favorable I−D interaction.

A second possible reason for the lack of tricontinuous microemulsion formation is the high molecular weight of the SID triblock, which prevents the blend from forming a homogeneous disordered phase at experimentally tractable temperatures. The Lifshitz point used to predict the approximate composition of a microemulsion is located at the phase boundary between disordered, ordered, and liquid phases, so accessing the disordered phase might be important in achieving a microemulsion that is, the microemulsion channel might not extend to the intermediate segregation strength that characterizes our system. By lowering the molecular weight of the triblock copolymer, disordered regions can be made experimentally accessible.

Finally, the homopolymer-to-triblock molecular weight ratio in the SID/S/D system is 0.05, for which Bates and Fredrickson predict swollen lamellar phases.[14] Tricontinuous microemulsions are predicted near the Lifshitz point located at 0.81 total homopolymer volume fraction for blends with a homopolymer-to-triblock molecular weight ratio of $\alpha = 0.2$ when the composition of the triblock copolymer is 0.2/0.6/0.2. Although the complex phases present in the SID/S/D system suggest that the morphologies are strongly influenced by the asymmetric χ parameters, increasing the homopolymer to triblock molecular weight ratio might also be important in the formation of a tricontinuous microemulsion.

Acknowledgment. Support for this research was provided by the NSF (DMR-9905008 and the MRSEC at the University of Minnesota) and by Lockheed Martin Energy Research Corporation (DOE Prime). M.S. also derived support from the Ministry of Education, Science, Sports and Culture of Japan under the fellowship program for university teachers for study abroad, and M.E.V. was supported in part by the Carlsberg Foundation, Denmark, and the Danish Technical Research Council. The authors thank Bryan Carlson of the University of Minnesota and Jim Hoffman of the University of California, Berkeley, for the implementation of TEMSIM at the University of Minnesota.

References and Notes

(1) Khandpur, A. K.; Foster, S.; Bates, F. S.; Hamley, I. W.; Ryan, A. J.; Bras, W.; Almdal, K.; Mortensen, K. *Macromolecules* **1995**, *28*, 8796.

(2) Matsen, M. W.; Bates, F. S. *J. Chem. Phys.* **1997**, *106*, 2436.

(3) Park, M.; Harrison, C.; Chaikin, P. M.; Register, R. A.; Adamson, D. H. *Science* **1997**, *276*, 1401.

(4) Discher, B. M.; Won, Y.-Y.; Ege, D. S.; Lee, J. C.-M.; Bates, F. S.; Discher, D. E.; Hammer, D. A. *Science* **1999**, *248*, 1143.

(5) Chan, V. Z.-H.; Hoffman, J.; Lee, V. Y.; Iatrou, H.; Avgeropoloulos, A.; Hadjichristidis, N.; Miller, R. D.; Thomas, E. L. *Science* **1999**, *286*, 1716.

(6) Matsen, M. W.; Bates, F. S. *Macromolecules* **1996**, *29*, 1091.

(7) Spontak, R. J.; Smith, S. D.; Ashraf, A. *Macromolecules* **1993**, *26*, 956. Zhao, J.; Majumdar, B.; Schulz, M. F.; Bates, F. S.; Almdal, K.; Mortensen, K.; Hajduk, D. A.; Gruner, S. M. *Macromolecules* **1993**, *29*, 1204.

(8) Shefelbine, T. A.; Vigild, M. E.; Matsen, M. W.; Hajduk, D. A.; Hillmyer, M. A.; Cussler, E. L.; Bates, F. S. *J. Am. Chem. Soc.* **1999**, *121*, 8457.

(9) Tanaka, H.; Hasegawa, H.; Hashimoto, T. *Macromolecules* **1991**, *24*, 240. Wang, K. I.; Thomas, E. L.; Fetters, L. J. *Macromolecules* **1992**, *25*, 422.

(10) Matsen, M. W. *Macromolecules* **1995**, *28*, 5765. Matsen, M. W. *Phys. Rev. Lett.* **1995**, *74*, 4225.

(11) Washburn, N. W.; Lodge, T. P.; Bates, F. S. *J. Phys. Chem. B* **2000**, *104*, 6987.

(12) Kahlweit, M.; Strey, R. *Angew. Chem., Int. Ed. Engl.* **1985**, *24*, 654.

(13) Bates, F. S.; Maurer, W. W.; Lipic, P. M.; Hillmyer, M. A.; Almdal, K.; Mortensen, K.; Fredrickson, G. H.; Lodge, T. P. *Phys. Rev. Lett.* **1997**, *79*, 849.

(14) Fredrickson, G. H.; Bates, F. S. *Eur. Phys. J.* **1998**, *B 1*, 71.

(15) Zheng, W.; Wang, Z.-G. *Macromolecules* **1995**, *28*, 7215.

(16) Auschra, C.; Stadler, R. *Macromolecules* **1993**, *26*, 2171. Krappe, U.; Stadler, R.; Voigt-Martin, I. *Macromolecules* **1995**, *28*, 4558. Breiner, U.; Krappe, U.; Abetz, V.; Stadler, R. *Macromol. Chem. Phys.* **1997**, *198*, 1051. Breiner, U.; Krappe, U.; Jakob, T.; Abetz, V.; Stadler, R. *Polym. Bull.* **1998**, *40*, 219.

(17) Brinkmann, S.; Stadler, R.; Thomas, E. *Macromolecules* **1998**, *31*, 6556.

(18) Mogi, Y.; Nomura, M.; Kotsuji, H.; Ohnishi, K.; Matsushita, Y.; Noda, I. *Macromolecules* **1994**, *27*, 6755.

(19) Matsushita, Y.; Suzuki, J.; Seki, M. *Physica B* **1998**, *248*, 238. Suzuki, J.; Seki, M.; Matsushita, Y. *J. Chem. Phys.* **1999**, *112*, 4862.

(20) Hückstädt, H.; Goldacker, T.; Göpfert, A.; Abetz, V. *Macromolecules* **2000**, *33*, 3757.

(21) Abetz, V.; Goldacker, T. *Macromol. Rapid Commun.* **2000**, *21*, 16.

(22) Breiner, U.; Krappe, U.; Thomas, E.; Stadler, R. *Macromolecules* **1998**, *31*, 135.

(23) $\chi_{SI} = 33.0/(T - 0.0228)$: Hashimoto, T.; Ijichi, Y.; Fetters, L. J. *J. Chem. Phys.* **1988**, *89*, 2463.

(24) $\chi_{ID} = 43.6/(T - 0.010)$, $\chi_{SD} = 68.0/(T + 0.037)$: Almdal, K. Danish Polymer Centre, Risoe National Laboratory, Roskilde, Denmark. Private correspondence.

(25) Ndoni, S.; Papadakis, C. M.; Bates, F. S.; Amdal, D. *Rev. Sci. Instrum.* **1995**, *66*, 1090.

(26) Rosedale, J. H. Ph.D. Thesis, University of Minnesota, Minneapolis, MN, 1993.

(27) Fetters, L. J.; Lohse, D. J.; Richter, D.; Witter, T. A.; Lukel, A. *Macromolecules* **1994**, *27*, 4639.

(28) Hajduk, D. A.; Harper, P. E.; Gruner, S. M.; Honeker, C. C.; Kim, G.; Thomas, E. L.; Fetters, L. J. *Macromolecules* **1994**, *27*, 4063.

(29) Lauer, J. H.; Hajduk, D. A.; Fung, J. C.; Sedat, J. W.; Smith, S. D.; Grunder, S. M.; Agard, D. A.; Spontak, R. J. *Macromolecules* **1997**, *30*, 3938. Avgeropolous, A.; Dair, B. J.; Hadjichristidis, N.; Thomas, E. L. *Macromolecules* **1997**, *30*, 5634.

(30) Vigild, M. E.; Almdal, K.; Mortensen, K.; Hamley, I. W.; Fairclough, J. P. A.; Ryan, A. J. *Macromolecules* **1998**, *31*, 5702.

(31) Detailed information about TEMSIM is available at the Web site http://www.msri.org/publications/sgp/jim/software/temsim.
(32) Gido, S. P.; Schwark, D. W.; Thomas, E. L.; Goncalves, M. C. *Macromolecules* **1993**, *26*, 2636.
(33) Lescanec, R. L.; Fetters, L. J.; Thomas, E. L. *Macromolecules* **1998**, *31*, 1680.
(34) Shefelbine, T. A. Ph.D. Thesis, University of Minnesota, Minneapolis, MN, 2001.